Research Article GU J Sci 38(2): 792-806 (2025) DOI: 10.35378/gujs.1474729

Gazi University

Journal of Science

http://dergipark.gov.tr/gujs

A Comparative Study of Two Types of Axial Flux Generators Associated with a Wind Turbine Prototype Using 3D FEM

Boubakar FARADJI [1,*], Aissa AMEUR [2]

[1]*University Amin Al-Akkal Haj Moussa Akhamok Tamanghesset, Faculty of science and technology, BP 10034, Route de l'aéroport Tamanghesset, Algeria*
[2]*University Amar Télidji Laghouat, Faculty of Technology, BP 37G route de Ghardaia, Laghouat, Algeria*

Highlights

- This paper focuses on axial flux permanent magnet generators study and realization.
- Production of electrical power from vertical and horizontal wind turbine.
- A highly three-dimensional finite element analysis accuracy calculation.

Article Info

Received: 28 Apr 2024
Accepted: 20 Jan 2025

Keywords

Single-side AFPMG
Double-side AFPMG
Wind Turbine
Prototype
Finite Element Method

Abstract

This research focuses on harnessing wind energy in remote areas to generate electricity using specialized wind turbines. A comparative study was carried out between two types of turbines—vertical and horizontal—to produce small-scale electrical energy. To facilitate this study, prototypes of both turbine types were developed and tested in the research laboratory. The electrical generators employed were Axial Flux Permanent Magnet Generators (AFPMG), which included two variants: single-side AFPMG and double-side AFPMG.

Given the working principles of axial flux generators, three-dimensional simulations utilizing finite element analysis were performed to monitor variations in the magnetic field across all directions. In the next phase of the research, fully assembled turbines underwent initial testing, with their performance compared against each other. The results of these experiments were analyzed comparatively, leading to several important findings that contribute valuable insights to this domain.

1. INTRODUCTION

In recent years, advanced scientific research has increasingly focused on renewable energy production derived from a variety of natural and sustainable sources. A key metric for evaluating and optimizing these energy sources is the power efficiency ratio, which serves as a benchmark for both acceptance and improvement.

In the context of wind energy systems, the power coefficient, which represents a wind turbine's power output ratio, plays a crucial role in classifying wind conversion systems whether vertical-axis, horizontal-axis, or other specialized designs. However, the design and operation of wind turbine technology are constrained by factors such as their electrical power capacity, operational range, and overload endurance at the generator level.

When megawatt-scale wind turbines are connected to the electrical grid to support heavy industrial loads, it becomes essential to implement optimal control strategies to regulate the generated power effectively. Research indicates that wind turbines can be equipped with various types of generators depending on their required capacity and application. For instance, these include Induction Generators (IG) with a capacity of 1,5 MW [1], Double-Fed Induction Generators (DFIG) with a 25 MW capacity [2], or Permanent Magnet

*Corresponding author, e-mail: boubakarluck@yahoo.fr

Synchronous Generators (PMSG) rated for 10 MW [3]. These systems are commonly controlled using Maximum Power Point Tracking (MPPT) algorithms to achieve optimal energy performance [4-6].

On the other hand, for small-scale operations such as individual farms or isolated installations, the power requirements are significantly lower compared to industrial-grade systems. In such cases, passive pitch control is generally sufficient for maximizing performance in kilowatt-scale wind turbines. For these smaller setups, it is advisable to design turbines using Direct Current (DC) generators or Permanent Magnet (PM)-based generators [7-12]. This is because almost all turbine performance metrics at this scale are directly linked to the optimization of generator design.

Permanent magnet synchronous rotating machines are broadly categorized into three well-known groups: Radial Flux Machines, Axial Flux Machines, and Transverse Flux Machines. Each of these groups offers distinct technical advantages tailored to specific applications [13-15]. Among these, the Axial Flux Permanent Magnet Motor (AFPMM) has garnered significant attention due to its versatile design potential and performance capabilities.

AFPMM topologies can be configured with varying electrical and magnetic parameters. Electrical variations stem from how the circuit coils are arranged, while magnetic characteristics depend on the design of the magnetic circuit and the geometric shapes of the permanent magnets, which may be circular, rectangular, or other forms. These motors are particularly valued for their high torque and power density, making them a preferred solution in traction applications [16,17]. Specifically, AFPMMs are frequently employed as wheel motors in both fully electric and hybrid electric vehicles (EVs), where their compatibility with the axial wheel form addresses critical space constraints [18-20].

A key design feature of AFPMMs is achieving a high torque-to-volume ratio while managing challenges such as Irreversible Demagnetization (ID) at elevated temperatures and increased torque ripple caused by rising motor current levels. These factors significantly impact the overall performance of the machine. To address these issues, studies such as those referenced in [21-24] focus on temperature management in AFPMMs, while investigations into the ID phenomenon and potential industrial solutions are explored in [25].

Additionally, similar AFPMM configurations are applied in direct-drive systems for wind turbine generators. Axial Flux Permanent Magnet Generators (AFPMGs) continue to be a focal point of research due to advancements in rare-earth materials used in permanent magnets. These new materials exhibit improved properties, enabling innovations such as the development of next-generation axial flux generators with exceptional performance, as highlighted in [26-30].

The highlighted performance parameters for all generators focus on six key aspects: flux density distribution, on-load terminal induced voltage (or back EMF), voltage regulation, harmonic distortion (THD coefficient), output power range (both active and reactive), and generator efficiency.

This leads us to the primary goal of the study: the design and development of two wind turbine prototypes tailored for isolated locations [31,32]. The first prototype is a three-bladed horizontal wind turbine, equipped with a single-sided axial flux permanent magnet generator (AFPMG). The second is a modified vertical MAGLEV wind turbine, incorporating a double-sided AFPMG. Both generators share the same outer diameter and use identical permanent magnet materials.

To support this research, a three-dimensional magnetic model using Finite Element Analysis (FEM3D) was developed. This analysis was conducted with FLUX 3D software supplied by CEDRAT, running on a computer with 8GB of RAM and a 1.6 GHz five-core processor. The simulation results for both generators under static conditions were analyzed and compared. Prototype construction took place in the Electrical Engineering Laboratory at the University of TAMANGHASSET, ALGERIA.

Initial experimental tests were carried out, yielding significant findings from the observed variations in induced voltage. These results provided valuable insights into the performance of both prototypes.

2. THE AFPMG GENERATOR DESCRIPTION AND MODEL

2.1. The AFPMG Description

When the induced magnetic flux path runs parallel to the rotor axis, a basic electromagnetic converter can be constructed using two discoid components. These components consist of ferromagnetic steel with windings that are dispersed, concentric, or toroidal, forming the stator or stationary part of the system. The movable component, referred to as the disc rotor, includes a shaft supported by rolling bearings, allowing it to rotate freely. The stator and rotor poles can be made from soft magnetic materials or standard magnetic sheets arranged axially. Both the stator and rotor are designed with the same number of poles and identical pole widths.

Figure 1(a) illustrates a single-sided axial flux permanent magnet generator (AFPMG), which features one stator and one rotor. This configuration is relatively straightforward but introduces a strong attractive force between the rotor and stator. To counteract this force and prevent axial movement of the rotor, a specialized thrust bearing is required, adding complexity to the design. Achieving a balanced force necessitates placing permanent magnet poles on the opposite side of the rotor, generating the magnetic field needed for stabilization. However, when the magnetic field oscillates, hysteresis and eddy current losses can occur as the stator laminates. By carefully designing the flux path, the force generated between the rotor and an additional stator can offset the force between the rotor and the slotted stator of the machine.

The double-sided AFPMG with an axial rotor, shown in Figure 1(b), is similar in design to its single-sided counterpart but differs by incorporating a second stator equipped with windings. Instead of relying on symmetry for balance in the single-sided version, this structure utilizes an additional stator to create a pathway for the magnetic field needed for force balancing. To accommodate this, the stator yoke length must be increased. Although this design offers better flux balance, it requires more materials compared to the single-sided configuration, resulting in higher material consumption.

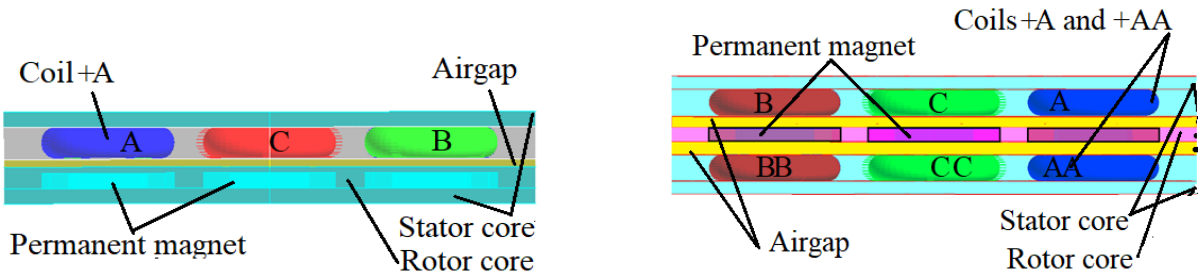

Figure 1. *Designed AFPMG cross section of (a) single-side (b) double-side*

The precise geometric features of the AFPMG for a single pole are illustrated in Figures 2(a), (b), and (c). These figures detail the one-sided stator, the single-sided rotor, and the double-sided rotor, all defined by a $2\pi/6$ spatial angle. The stator winding is composed of a mover equipped with permanent magnets (PMs) and a steel pole, along with a stator featuring a coreless three-phase winding.

The magnetic topology comprises iron poles and circular ring PMs that are axially magnetized, forming a magnetic flux pathway. As PMs are easy to magnetize, this design approach allows for the creation of particle topology at a lower production cost.

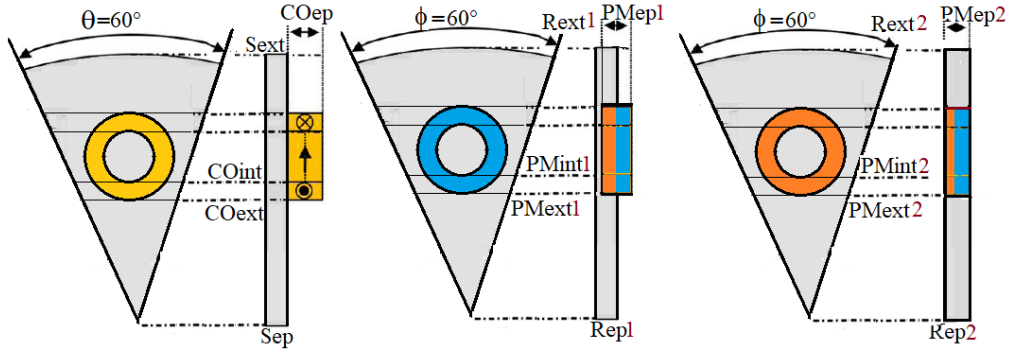

(a) *(b)* *(c)*

Figure 2. *Specific geometrical parameters in the AFPMG apparatus* (a) *Single-side stator (b) Single-side rotor (b) Double-side rotor*

The data design differences for the stator and rotor in a single-side AFPMG and a double-side AFPMG are displayed in Table 1. The AFPMG estimated electrical power is 500Watt.

Table 1. *The Detailed geometry parameters in Single-side and double-side AFPMG*

parameter	Description	value	Unite	Parameter	Description	Value	Unite
AFPMG Stator				**Permanent Magnet**			
Sext	Outer diameter of Stator	120	mm				
				PMext1,2	Magnet outer rayon	18	mm
Sep	Stator yoke thickness	5	mm	PMint1,2	Magnet inter rayon	10	mm
θ	Stator pole opening	60	Degree	PMep1,2	Magnet thickness	6	mm
E	Airgap	1	mm	Magnets	Magnets number	6	
L	Stator length	40	mm		**Stator coil**		
Single-side and double-side AFPMG rotor				COext	Coils outer rayon	20	mm
Rext	Outer rotor rayon	100	mm	COint	Inner diameter of Coil	10	mm
Rep1	Rotor yoke thickness	6	mm	COep	Coils thickness	8	mm
Rep2	Rotor yoke thickness	6	mm				
ϕ	Rotor pole opening	60	mm	N	Coils turns	90	
				Wire	Coil wire section	0.63	mm^2
				Coils	Coils number	6	

Figures 3(a) and 3(b) illustrate the winding association circuit for single-sided and double-sided AFPMG configurations, respectively. To minimize magnetic flux loss, the internal profile of the coil is designed to closely match the size and shape of the magnets used. In single-sided AFPM generators, six coils are arranged in a star configuration, while in double-sided AFPMGs, the total number of coils increases to 12. Figure 3 provides a visual representation of how these coils are interconnected.

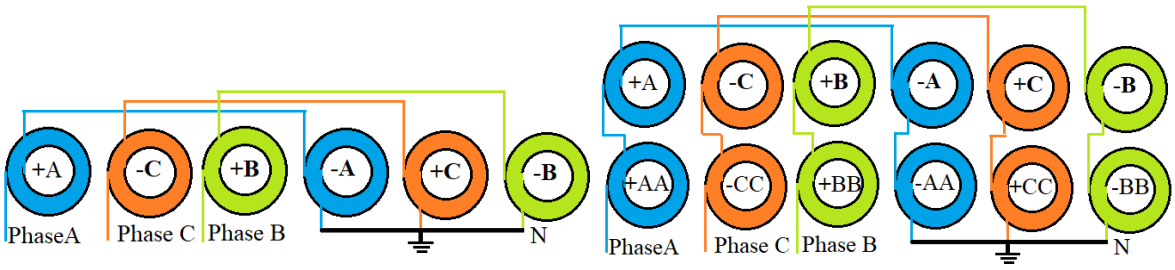

(a) *(b)*

Figure 3. *Detailed Coils connection in AFPMG* (a) *Single-side rotor (b) Double-side rotor*

2.2. The AFPMG Electromagnetic Model

In order to calculate the magnetic field, the AFPMG is modelled using the 3DFEM approach. One can construct a general equation by using Maxwell's Equations (1). Additionally, due to the lack of free current in the PM region:

$$\begin{cases} \overrightarrow{rot}\,\vec{H} = 0 \\ \vec{B} = \mu_0(\vec{H} + \vec{M}) \\ \overrightarrow{rot}\vec{B} = \mu_0(\vec{H} + \vec{M}) \end{cases} . \quad (1)$$

The magnetic vector potential A is defined as Equation (2):

$$\overrightarrow{rot}\vec{A} = \vec{B} \quad . \quad (2)$$

Equation (3) illustrates how the governing equations in the region of air are expressed using Laplace's formula. Using Poisson's equations, the PM region's governing equation is expressed as (3) :

$$\begin{cases} \nabla^2\vec{A} = 0 \\ \nabla^2\vec{A} = -\mu_0(\overrightarrow{rot}\,\vec{M}) \end{cases} . \quad (3)$$

Using the concept of the magnetic vector potential and the answers to the governing equations in (3)

μ_0: The permeability of free space
$\vec{J}$: Current density
$\vec{H}$: Magnetic field intensity
$\vec{B}$: Magnetic flux density
$\vec{A}$: Magnitec potential vector
μ: Magnetic permability
$\vec{M}$: Magnetization vector of the PM.

The finite element method is used to solve the equation defining the domain study's boundary conditions Dirichlet and Neumann (FEM).

- Dirichlet boundary conditions in magnetic problems is to define $A = 0$ along a boundary to keep magnetic flux from crossing the boundary.
- Neumann boundary condition, $\partial A/\partial n = 0$ is defined along a boundary to force flux to pass the boundary at exactly a 90^o angle to the boundary.

3. THE NUMERICAL MODEL SALVATION METHOD PRINCIPLE

For addressing non-linear electromagnetic problems through finite element analysis (FEA), the commercial software FLUX3D is employed. FLUX3D comprises around ten different programs or commands, each tailored to perform specific functions such as geometry and mesh definition, circuit description, physical property assignment, problem resolution, results analysis, and more.

The axial flux permanent magnet generator (AFPMG) under consideration, as illustrated in Figure 1, features a straightforward and classical design. It is configured as a six-pole, single-sided generator with two-phase coils and six concentric coils. Alternatively, the double-sided generator variant comprises four coils per phase, totaling twelve coils. In all configurations, the rotor accommodates six permanent magnets (PMs).

To address the governing equation, three primary steps are required: defining the geometry, meshing the geometry, and analyzing the simulation results. Figures 4(a) and 4(b) present the geometry of the AFPMG within the Flux3D environment for the double-sided and single-sided configurations, respectively.

Table 1 details all components included in the simulation such as the air gap, stator, rotor, permanent magnets, and non-meshed coils which are assigned both geometric and magnetic properties. When defining a motor's geometry using FLUX3D in a conventional approach, important tasks include determining the coordinates of points and lines, as well as specifying mesh densities.

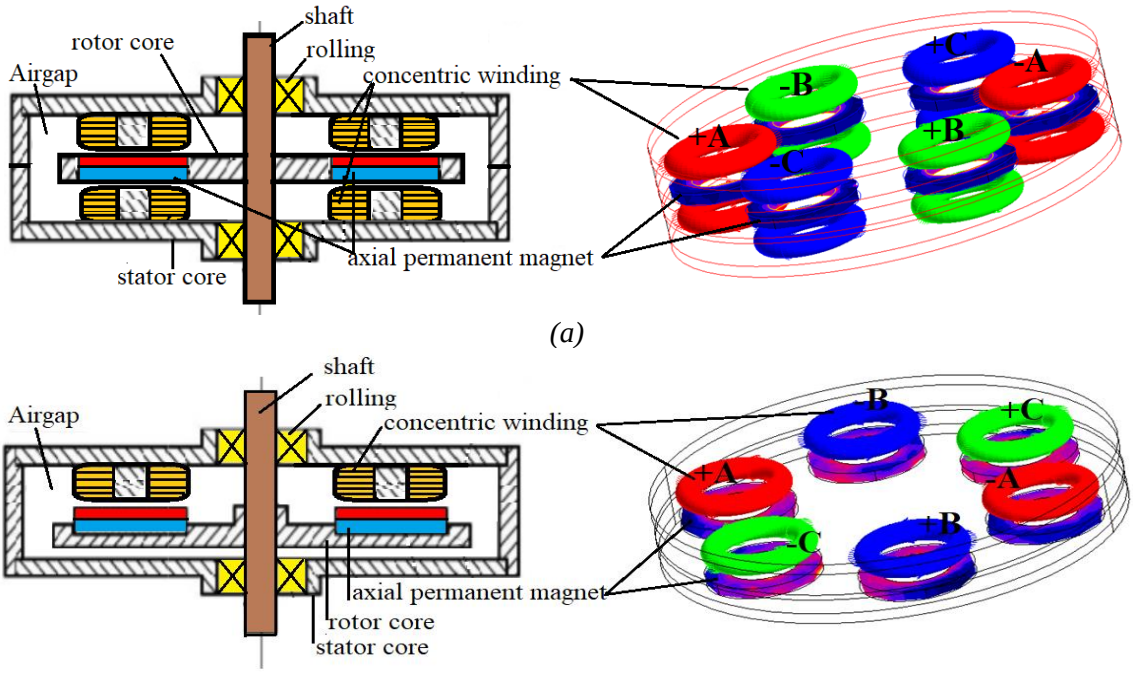

Figure 4. *The detailed AFPMG structure and the Flux3D environment's AFPMG over view geometry of (a) Double-side (b) Single-side*

Electromagnetic energy concentration in this region causes the mesh to be denser near the air gap. However, to reduce computation times without significantly compromising accuracy, a coarser mesh is applied along the shaft's direction and outside the cylinder head.

The 3D generator mesh, illustrated in Figures 5(a) and 5(b), comprises 79,823 nodes for the double-sided AFPM and 7,663 nodes for the single-sided AFPM. The magnetic flux utilizes the teeth and stator slots as its primary path, resulting in a higher mesh density in both the air gap and these areas. When incorporating sliding surfaces within the air gap, it is crucial to maintain a regular mesh in this region. Doing so prevents the need for re-meshing and offers significant time-saving advantages.

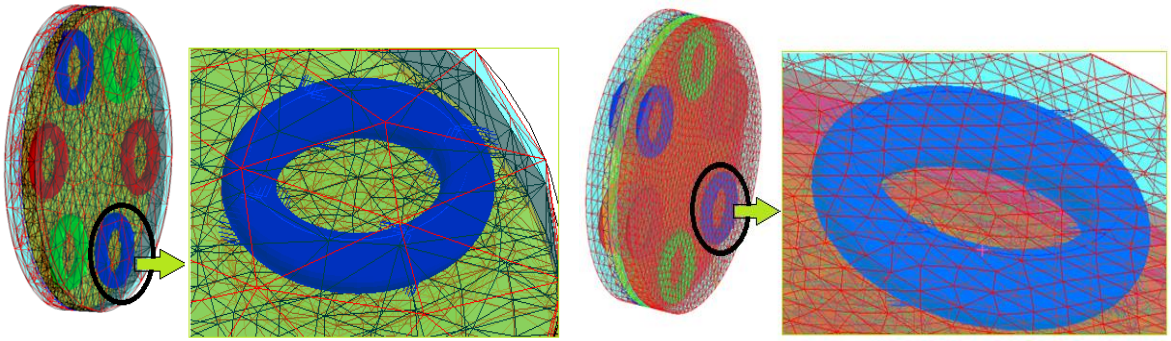

(a) *(b)*

Figure 5. *The AFPMG geometry3D mesh in the Flux3D environment (a) Single-side (b) Double-side*

4. SIMULATION RESULTS AND DISCUSSION

This section has presented a comparison of the proposed generators from a dimensional perspective; however, their performance has not yet been analyzed. The steady-state response is highlighted here to illustrate the general behavior expected from both single-side and double-side AFPMGs. A detailed analysis of each machine will be provided in the upcoming sections.

4.1. The AFPMG Stator Analyses

Under no-load conditions, the postprocessing phase involves analyzing the magnetic field distributions. The generator produces the flux density map displayed in Figures 6(a) and 6(b) for the single-sided AFPMG and double-sided AFPMG, respectively, using FEM 3D resolution. The flux density distribution reveals that saturation occurs in most areas of the stator core, although the values remain within the acceptable limit of 1.8T. Concentration of the flux density is observed where the stator coils are positioned on the stator core. In the case of the single-sided stator armature, the flux density is intense across all sides of the coils. Conversely, for the double-sided configuration, the flux exhibits a symmetrical distribution across both sides of the stator, with zero-intensity regions occurring at the midpoint of each stator coil and at the center of the stator.

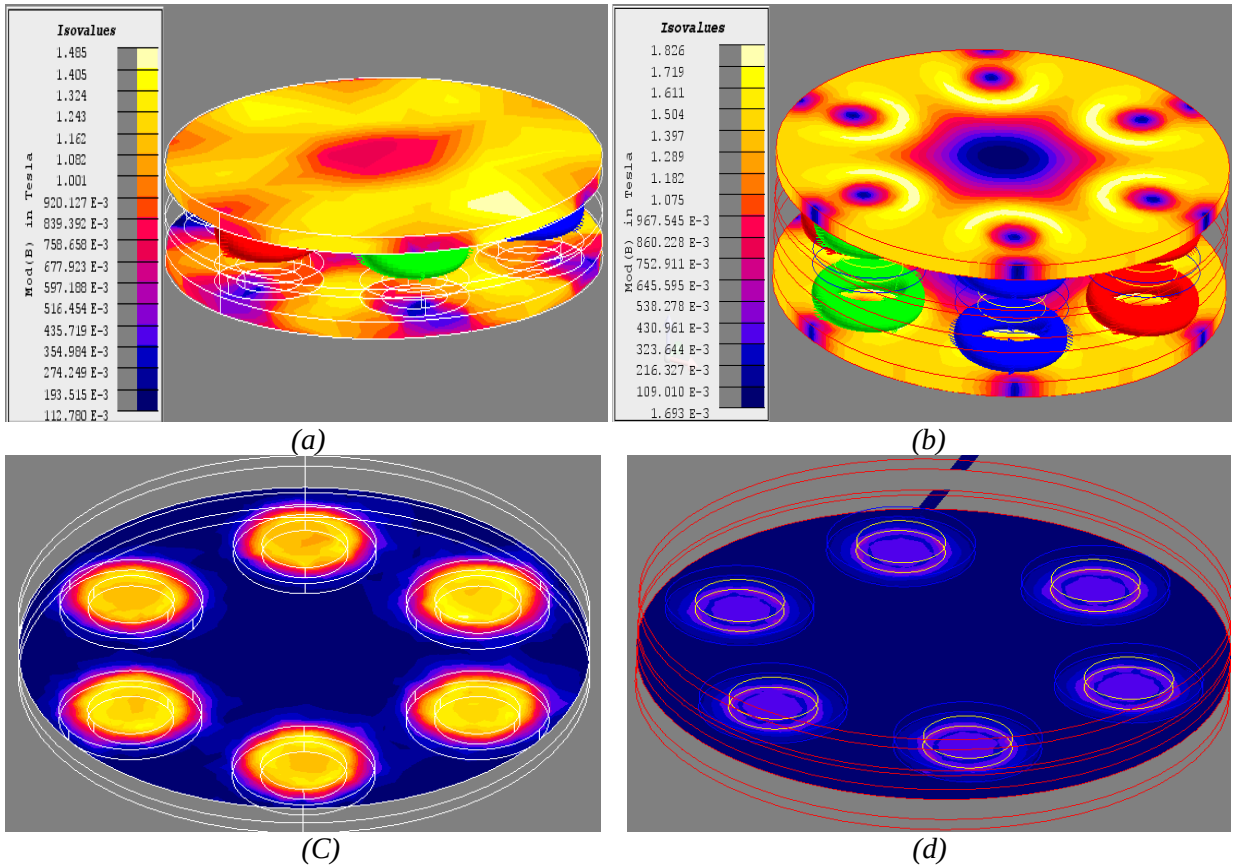

Figure 6. *The AFPMG flux density map of (a) Single-side in stator (b) Double-side in stator(C) Single-side under PM in rotor (d) Double-side in stator under PM in rotor*

Figures 7(a) and 7(b) illustrate the magnetic flux patterns within the stator armature for single-side and double-side axial flux permanent magnet generators (AFPMGs), respectively. These plots reveal the radial flux composite fluctuations. The flux values along each path align with the flux density map provided in Figure 6(a). Notably, the circulation of flux paths in the double-sided generator forms nearly complete circles, with enhanced distribution around the stator coil areas. Conversely, in the single-side AFPMG, the flux density map indicates weaker reinforcement and increased disruption on both stator sides, as observed in the flux route patterns within the stator.

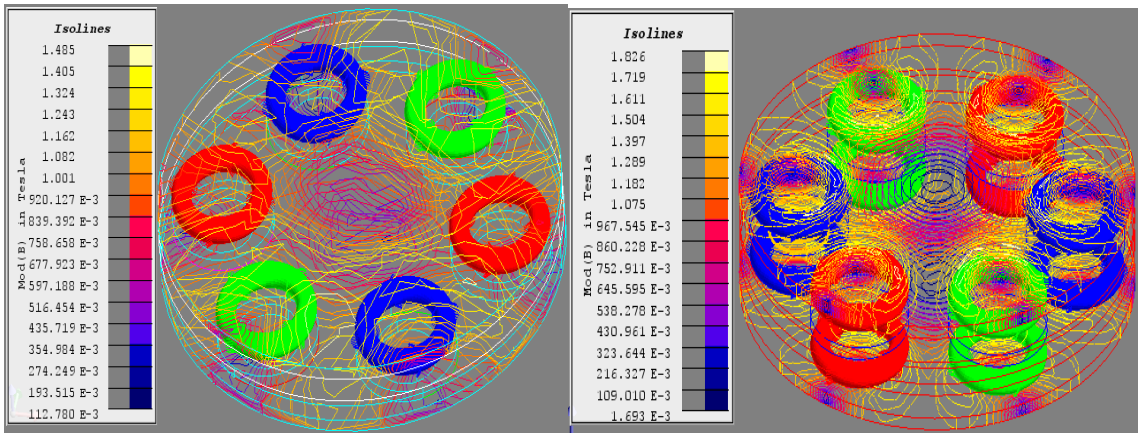

(a) *(b)*

Figure 7. *The AFPMG magnetic flux paths (a) Single-side (b) Double-side*

In the single-sided AFPMG configuration with a zoomed view of two adjacent stator coils depicted in Figure 8(b), the three-dimensional flux density directions can be observed in Figure 8(a). These figures illustrate the axial flux variation in the system. Figure 8(c) presents the double-sided AFPMG, with a more focused zoom provided in Figure 8(d). When two adjacent coils exhibit differing flux directions, the magnetic flux generated within the air gap by the rotor permanent magnets (PMs) in the generating coils aligns with the polarity of the rotor PMs.

In Figure 8(b), the flux input direction is indicated by point AA in the first magnification, while point BB represents the output direction. The primary flux line forms an elliptical circulation path between these two points, though the alternative flux route within the stator core is noticeably less structured. In Figure 8(d), which provides a second magnified view, two additional points are marked: point CC signifies the flux input direction, while point DD represents the output. Here, the overall flux paths between the air gap and the stator core are more organized, as nearly all flux arrows close in pathways connecting the four stator coils.

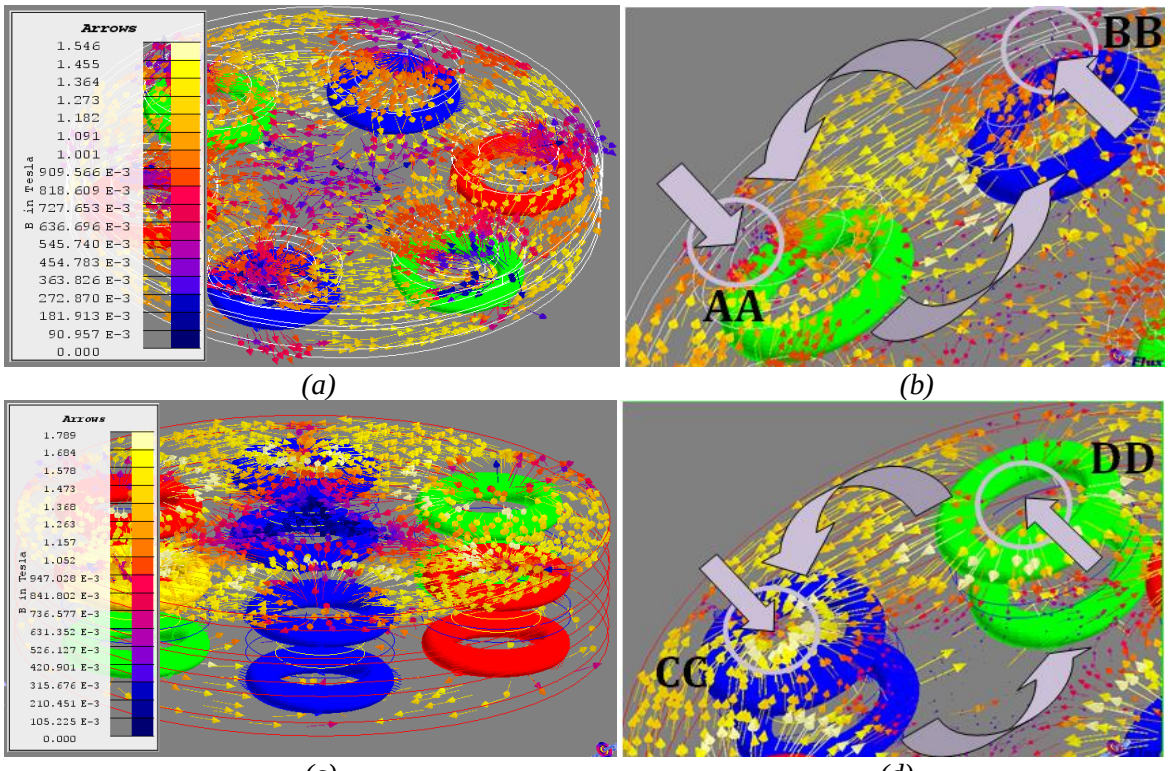

(c) *(d)*

Figure 8. *The AFPMG flux density arrows (a) Single-side (b) Double-side*

Figures 9(a) and 9(b) illustrate a complete generator pole for single-sided and double-sided AFPMGs, respectively. Both configurations feature six poles on the stator and rotor. The diagrams provide a view of the flux paths within the rotor's permanent magnets (PMs) and a cross-sectional perspective of the stator armature. In the double-sided AFPMG, where the maximum flux value is consistent, the PM flux transitions outward from the inner magnetic flux paths to form fully closed circular routes. By contrast, in the single-sided generator, the PM flux lines are more dispersed within the rotor core, and the resulting circular flux paths remain partially open.

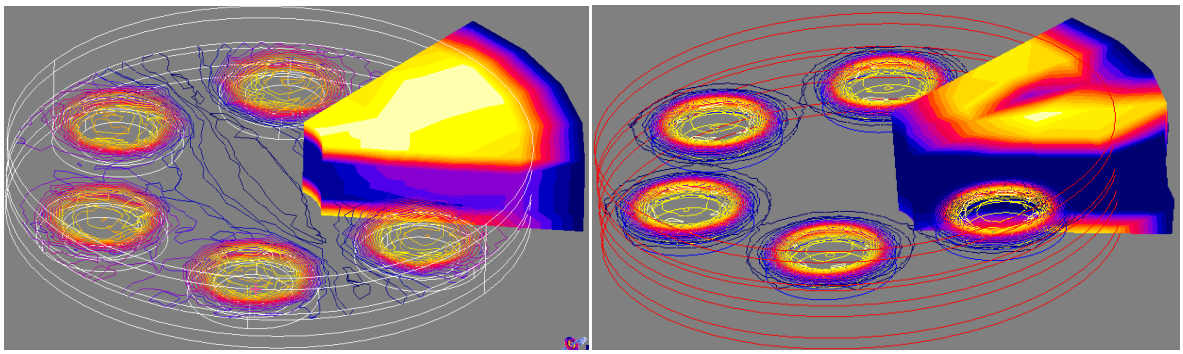

(a) *(b)*

Figure 9. *The AFPMG cross-section for stator armature flux density and rotor PMs flux paths of (a) Single-side (b) Double-side*

4.2. The AFPMG Rotor Analyses

Figures 10(a) and 10(b) present the outcomes of the 3D FEM analysis of the rotor PMs in the generator, illustrating the magnetic flux density for both the single-sided and double-sided generators. For the double-sided configuration, the flux density remains uniform across all rotor PMs. The internal surface of the PMs, corresponding to the primary magnetic flux path depicted in Figure 9(a), exhibits the highest flux density. This peak value occurs when the flux directions in the rotor core and the PM align. Conversely, in the single-sided case, the flux density distribution among the PMs shows slight variations, influenced by their respective positions on the rotor.

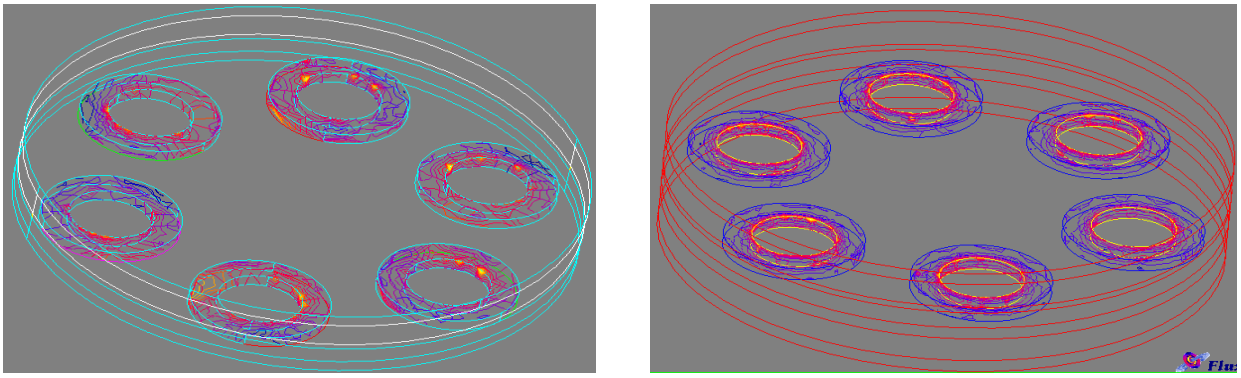

(a) *(b)*

Figure 10. *The AFPMG* flux *density in rotor PMs (a) Single-side (b) Double-side*

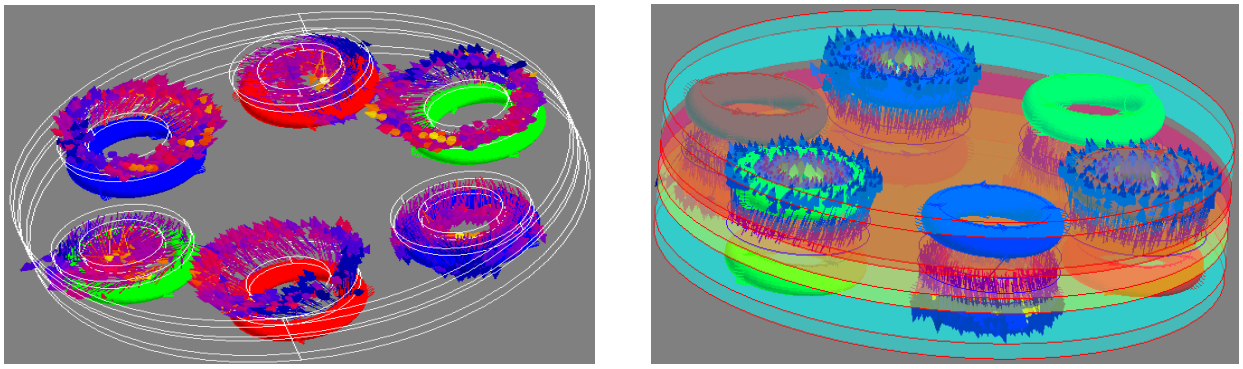

(a) *(b)*

Figure 11. *The AFPMG flux density arrows in rotor PMs (a) Single-side (b) Double-side*

Figure 11(a) illustrates the PM flux density arrows in the single-sided AFPMG, aligned with the axial rotational direction of the shaft. When the PM polarization is directed from the air gap toward the stator, the arrows exhibit a slight inward tilt. Conversely, if the polarization is reversed, the tilt shifts outward. In contrast, as depicted in Figure 11(b), the PM flux density arrows in a double-sided AFPMG are fully axial, maintaining a perpendicular alignment with the rotor core.

5. EXPERIMENT TESTS RESULTS AND DISCUSSION

A comparative analysis has been conducted between a three-phase, single-sided AFPMG and a three-phase, double-sided AFPMG to evaluate and validate their performance characteristics. The data, derived through FEM analyses, supports the findings outlined in the research.

The experimental setup includes two wind turbine prototypes designed in the university laboratory for direct-drive operation. Figure 12(a) illustrates the single-sided AFPMG, which is integrated with a horizontal-axis wind turbine. The initial section of the diagram provides detailed information on the generator's design, including the materials used, dimensions, and performance ratings. Notably, the stator coils are arranged with external wire terminal connections, as shown in the final view of the generator's permanent magnet arrangement.

Figure 12(b) presents the vertical-axis wind turbine equipped with a double-sided AFPMG prototype. Both the design and fabrication processes for this generator were completed within the same laboratory. Similar to its single-sided counterpart, the coil terminals for this configuration are located externally, while its dual-stator coils maintain consistent generator characteristics.

To evaluate performance, a digital storage oscilloscope (DSO) was utilized to capture initial test results for back-EMF (induced voltage) at varying wind speeds. As depicted in Figure 12, two DSO probes were connected to the generator's phase terminals to record line-to-neutral and line-to-line back-EMF potentials. Wind speeds were measured using a min-anemometer positioned near the turbine and aligned with wind flow direction. The fabricated prototypes were tested under low wind speed conditions to monitor and analyze their performance.

(a) *(b)*

Figure 12. *An overview of the measurement set for the prototype generator test bench utilized in the study involving the two generator structures (a) Single-side AFPMG (b) Double-side AFPMG*

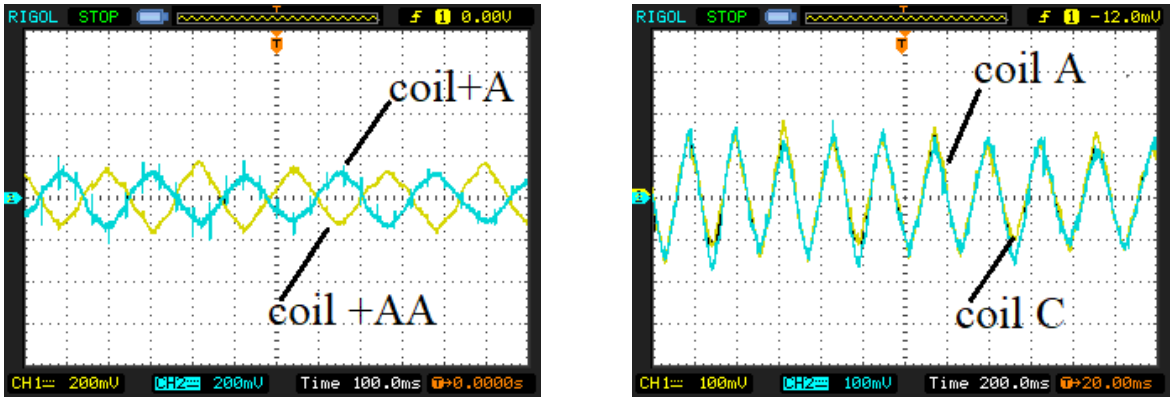

(a) *(b)*

Figure 13. *Observed double-side AFPMG voltage experimental findings (a) Two coils in opposite position for the same stator phase (200mV/div, 100ms/div) (b) Two coils in the same position for different stator sides(100mV/div, 200ms/div)*

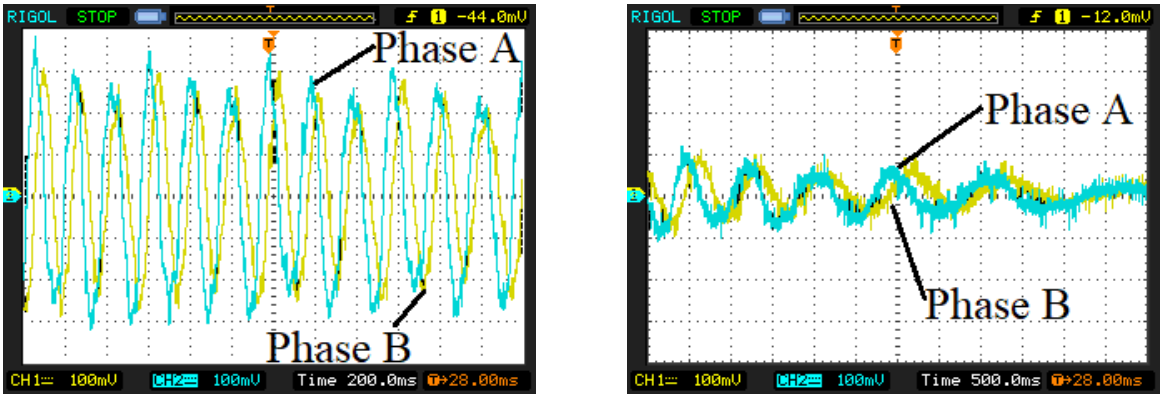

(a) *(b)*

Figure 14. *Observed experimental results of double-side AFPMG two-phase voltage (a) after a few seconds of start turbine rotation (100 mV/div, 500 ms/div) and (b) near stop turbine rotation (100 mV/div, 500 ms/div)*

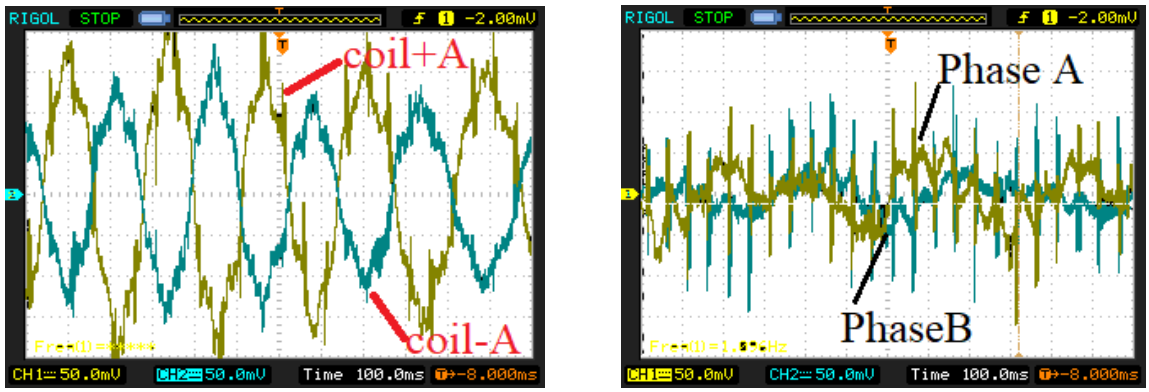

(a) *(b)*

Figure 15. *Observed experimental results of single-side AFPMG voltage (a) Two coils in opposite position for the same stator phase (50mV/div, 100ms/div) (b) Two phase voltage (50mV/div, 100ms/div)*

The 3D FEA simulation findings align well with the results obtained from experimental observations.

Figure 13(a) depicts the back-EMF in two separate coils positioned at opposite locations within the same stator phase (-A and +A) of a double-sided AFPMG. For each coil, the voltage is represented as a sinusoidal waveform over time. In contrast, Figure 13(b) shows the back-EMF for two coils situated in corresponding positions on either side of the stator phase (+AA and +A). Here, the voltage for each coil is illustrated as overlapping sinusoidal waveforms over time. When the back-EMF is influenced by wind speed, the recorded waveforms for the induced stator voltages in phases A and B are presented in Figures 14(a) and 14(b). Figure 15(a) displays the back-EMF in two separate coils positioned at opposite locations within the same stator phase (-A and +A) for a single-sided AFPMG. Similar to earlier cases, each coil's voltage is shown as a sinusoidal waveform over time. However, when compared to the double-sided AFPMG, the induced voltage in Figure 15(b), which illustrates the back-EMF across two phases, does not form a purely sinusoidal waveform. Instead, it contains significant harmonics and noticeable ripples.

4. CONCLUSION

Our research focuses on harnessing wind energy in remote areas, with both turbines demonstrating their effectiveness in this context, albeit with a slight edge for the horizontal turbine.

The initial phase of the study involved a three-dimensional simulation using a highly precise program. This tool allowed us to thoroughly analyze and compare key variables impacting generator efficiency by defining the orientation and distribution patterns unique to each variable during generator operation.

Following the simulation stage, a practical step was undertaken to construct both turbines. This phase demanded considerable effort to achieve these preliminary outcomes within the constraints of available resources.

In the final stage, preliminary experiments were conducted to validate key aspects such as operational principles, energy generation, voltage output characteristics, and the influence of varying coil connections.

Ultimately, this research holds significance as it enables a comprehensive comparison between two small-scale turbines, identifies critical factors affecting turbine efficiency, and underscores the importance and potential of vertical turbines as promising candidates for innovative applications.

CONFLICTS OF INTEREST

No conflict of interest was declared by the authors.

REFERENCES

[1] Vukadinović, D., and Bašić, M., "A stand-alone inductıon generator wıth improved stator flux orıented control", Journal of Electrical Engineering, 62(2): 65-72, (2011).

[2] Soued, S., Ramadan, H.S., and Becherif, M., "Effect of doubly fed induction generator on transient stability analysis under fault conditions", Journal of Energy Procedia, 162(1): 315-324, (2019).

[3] Stuebig, C., Seibel, A., Schleicher, K., Haberjan, L., Kloepzig, M., and Ponick, B., "Electromagnetic design of a 10 MW permanent magnet synchronous generator for wind turbine application", IEEE International Electric Machines & Drives Conference (IEMDC), Coeur d'alene ID USA, 10-13, (2015).

[4] Karthikeyan, S., and Ramakrishnan, C., "A hybrid fuzzy logic-based MPPT algorithm for PMSG-based variable speed wind energy conversion system on a smart grid", Journal Energy Storage and Saving, 3(4): 295-304, (2024).

[5] Hossam, H.H.M., Abdel-Raheem, Y., and Essam, E.M.M., "Modifed P&O MPPT algorithm for optimal power extraction of five-phase PMSG based wind generation system", Journal SN Applied Sciences, 1(838), (2019).

[6] Marwa, M., Ahmed, A., Wael, S., Hassanein, B., Nadia, A., Elsonbaty, C., and Mohamed, A., "Enany proposing and evaluation of MPPT algorithms for high-performance stabilized wind turbine driven DFIG", Journal Alexandria Engineering, 59(6): 5135-5146, (2020).

[7] Chen, Y.J., Tsai, Y.F., Huang, C.C., Li, M.H., and Hsiao, F.B., "The design and analysis of passive pitch control for horizontal axis wind turbine", Journal Energy Procedia, 61(1): 683-686, (2014).

[8] Gambuzza, S., Sunil, P., Felli, M., Anna, M. Y., Broglia, R., McCarthy, E. D., and Viola, I. M., "Power and thrust control by passive pitch for tidal turbines", Journal Renewable Energy 239(121921), (2025).

[9] Apata, O., and Oyedokun, D.T.O., "An overview of control techniques for wind turbine systems" Journal Scientific African, 10(e00566), (2020).

[10] Nurmalia, A., Hadi, W., and Cahyadi, W., "Performance test of three-phase brushless direct current motor axial flux with differences diameter of neodymium type permanent magnet", Journal ELKHA, 13(1), (2021).

[11] Nishanth, F., Verdeghem, J.V., and Severson, E.L., "A Review of axial flux permanent magnet machine technology", IEEE Transactions on Industry Applications, 59(4): 1-14, (2023).

[12] Ketut, W., and Chun-Yu, H., "Performances comparison of axial-flux permanent magnet et generators for small-scale vertical-axis wind turbine", Alexandria Engineering Journal, 61: 1201-1215, (2022).

[13] Bo, Z., Torsten, E., Martin, D., and Matthias, G., "A comparison of the transverse, axial and radial flux PM synchronous motors for electric vehicle", IEEE International Electric Vehicle Conference (IEVC), Florence,17-19, (2014).

[14] Hao, Z., Ma, Y., Wang, P., Luo, G., Chen, Y., "A review of axial-flux permanent-magnet motors: topological structures, design, optimization and control techniques", Journal MDPI Machines, 10(1178), (2022).

[15] Wang, H., Zeng, X., Eastham, J.F., and Pei, X., "Axial flux permanent magnet motor topologies magnetic performance comparison", Journal MDPI Energies, 17(401), (2024).

[16] Ebrahimi, H., Torkaman, H., and Javadi, H., "Simultaneous improvement of cogging torque and torque density in axial flux-switching permanent magnet motor", IET Electric Power Applications, 18(3): 312-324, (2024).

[17] Tayfun, G., "Torque capability comparison of induction and interior permanent magnet machines for traction", Gazi University Journal of Science, 36(2): 675-691, (2023).

[18] Credo, A., Tursini, M., Villani, M., Di Lodovico, C., Orlando, M., and Frattari, F., "Axial flux pm in-wheel motor for electric vehicles: 3D multiphysics analysis", Journal MDPI Energies, 14(2107), (2021).

[19] Hamza, A.S., Sajjad, H.Z., and Farhan, K., "A comparative study on different motors used ın electric vehicles", Journal of Independent Studies and Researc-Computing, 20(2), (2022).

[20] Agamloh, E., Jouanne, A.V., and Yokochi, A., "An overview of electric machine trends in modern electric vehicles", Journal MDPI Machines, 8(2): 20, (2020).

[21] Carlos, M.E., Danıel, H.P., Roberto, V.R., and Danıel, M.M., "Review of flux-weakening algorithms to extend the speed range in electric vehicle applications with permanent magnet synchronous machines", IEEE Access, (11): 22961-22981, (2023).

[22] Mahmouditabar, F., Vahedi, A., and Takorabet, N., "Demagnetisation optimisation of ring winding axial flux permanent magnet motor by modifying the load line of the magnet", IET Electric Power Applications, 17(7): 928-938, (2023).

[23] Mahmouditabar, F., Vahedi, A., and Takorabet, N., "Design and analysis of ınterior permanent magnet motor for electric vehicle application considering irreversible demagnetization" IEEE Transactions On Industry Applications, 58(1):284-293, (2022).

[24] Kurt, E., Demirci, M., and İlbaş, M., "Implementation of heat transfer techniques for an axial flux permanent magnet generator design", Proceedings of the Institution of Mechanical Engineers, Part A: Journal of Power and Energy, 238(6), (2024).

[25] Mahmouditabar, F., Vahedi, A., and Fabrizio, M., "The demagnetization phenomenon in PM machines: principles, modeling, and design considerations", IEEE Access, (11): 47750-47773, (2023).

[26] İlbaş, M., Demirci, M., and Kurt, E., "Modeling and experimental validation of flow phenomena for optimum rotor blades of a new type permanent magnet generator", Journal SN Applied Sciences, 1(12): 1544, (2019).

[27] Jianfei, Z., Xiaoying, L., Shuang, W., and Lixiao, Z., "Review of design and control optimization of axial flux PMSM in renewable-energy applications", Chinese Journal of Mechanical Engineering, 36(45), (2023).

[28] Ghaheri, A., Afjei, E. and Torkaman, H., "A novel axial air-gap transverse flux switching PM generator: design, simulation and prototyping", IET Electric Power Applications, 17(4): 452-463, (2023).

[29] Asiful, H., Hang, S.C., Nasrudin, R., Mahdi, T., and Erwan, S., "A fully coreless multi-stator multi-rotor (MSMR) AFPM generator with combination of conventional and halbach magnet arrays", Alexandria Engineering Journal, 59(2): 589-600, (2020).

[30] Jun, Z., Huaichun, N., Xiangwei, G., Penghui, L., Shaotong, D., and Ming, Y., "Design and optimization of a new half direct-driven mw-scale axial flux permanent magnet generator for wind turbine", Journal of Electrical Engineering & Technology, 18(1): 3671-3680, (2023).

[31] Faradji, B., and Ameur, A., "An axial flux generator for wind turbine in autonomous low-power production", Majlesi Journal of Electrical Engineering, 18(2): 1-7, (2024).

[32] Bharathi, M., Malligunta, K.K., and Udochukwu, B.A., "Design and performance assessment of a small-scale ferrite-PM flux reversal wind generator", Journal MDPI Energies, 15(2): 636, (2020).